Journal of the Korean Physical Society, Vol. 45, No. 4, October 2004, pp. 1065∼1068

Electroluminescence Properties of Nanocrystal Si/SiO_2 Superlattices Grown by Rapid Thermal Chemical Vapor Deposition

Jung Hyun KAANG, Young Dae KIM, Kyu Man CHA, Hea Jeong CHEONG, Yong KIM,* Jae-Yel YI, Hong Jun BARK and Tae Hun CHUNG

Department of Physics, Dong-A University, Busan 604-714

(Received 20 July 2004)

The electroluminescence (EL) properties of metal-oxide-semiconductor (MOS) devices employing nanocrystal Si/SiO_2 superlattices are investigated. The amorphous silicon-rich oxide/SiO_2 superlattices are grown by using rapid thermal chemical vapor deposition. During high-temperature annealing at 1100 °C, Si nanocrystals are precipitated. Despite the simple MOS structure, the device shows conventional diode behavior in the current-voltage characteristics. We observe EL only under the forward bias condition, and the turn-on voltage is as low as 8 V. The EL intensity increases with increasing bias and is saturated over 11 V. We observe a systematic blueshift of the EL with increasing applied bias. Therefore, the observed EL is attributed to radiative recombination of carriers confined in the Si nanocrystals.

PACS numbers: 78.55.-m, 78.67Bf, 68.37.Lp, 81.07.Bc
Keywords: Electroluminescence, Si nanocrystals, Photoluminescence, Rapid thermal chemical vapor deposition

I. INTRODUCTION

Since the first discovery of light emission from porous silicon [1], interest in Si-based optoelectronics has rapidly increased. Due to their better compatibility with standard ultra-large scale integrated circuit (ULSI) processes, Si nanocrystals in a dielectric matrix have gained much interest. The standard approach for the formation of Si nanocrystals is prolonged annealing of substoichiometric silicon oxide (*i.e.*, silicon-rich oxide, SRO) at temperatures higher than 900 °C [2]. During the annealing, phase separation and precipitation take place owing to the energetic stability of the Si and the SiO_2 phases [3]. Methods for the formation of substoichiometric silicon oxide include ion-implantation [4], plasma-enhanced chemical-vapor deposition (PECVD) [5], low pressure CVD (LPCVD) [6], reactive evaporation [7], co-sputtering [8], pulsed laser deposition [9], and electron cyclotron resonance CVD [10].

A rapid thermal chemical vapor deposition (RTCVD) apparatus has emerged as a next generation cluster tool for ULSI technology [11]. The growth by RTCVD proceeds via a limited reaction processing [12]. Thus, the RTCVD apparatus is inherently a single-wafer-based processing tool. In addition, since RTCVD is a cold wall process, a particulate-free ultra-thin layer is easily obtainable. Despite the importance of the RTCVD method, little work has been done specifically for the growth of SRO layers, except our recent report [13]. The fabrication of an electroluminescence (EL) device is of prime importance due to its application for future optical interconnections. However, reports concerning EL devices are limited due the difficulty in current injection via a diectric matrix [14]. Thereby, the turn-on voltage of EL emission usually exceeds 10 V [15]. Recently, Irrera *et al.* [16] reported an EL device with a turn-on volage as low as 4 V; the devices employed an ultra-thin active layer. In this research, we utilized the advantage of RTCVD to prepare reliable ultra-thin layers for efficient EL-device fabrication.

II. EXPERIMENTAL DETAILS

SRO and SiO_2 layers were grown by using a home-built RTCVD system. The processing gases were 20 % Ar-diluted SiH_4 and N_2O. A bank of tungsten-halogen lamps allows rapid heating of 3-inch Si wafers at the ramp rate of 80 °C/sec. The wafer temperatures, calibrated by using a thermocouple, were monitored with a infrared pyrometer (IRCON with 5-μm detection band) through a sapphire window. The Si wafers were inverted and supported by sharp quartz pins, and the source gases were injected from the bottom of the cold-wall reaction chamber. Such an inverted structure ensures minimal inclusion of particulates. The chamber pressure was maintained by using feedback from a MKS throttle valve and a Baratron gauge. The chamber pressure was kept at 2

*E-mail: yongkim@daunet.donga.ac.kr

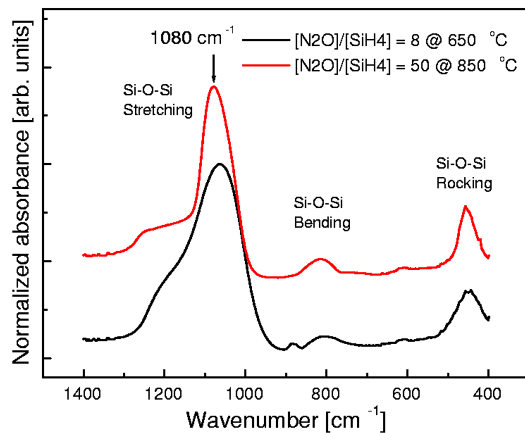

Fig. 1. FTIR spectra of SRO and SiO_2 layers.

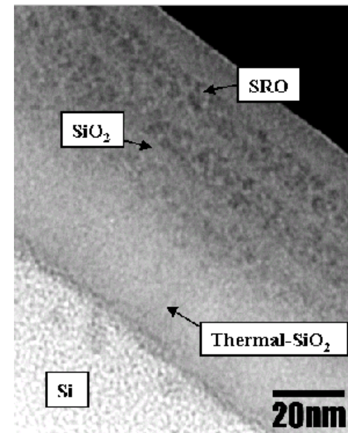

Fig. 2. Low-magnification cross-sectional TEM image of the EL device.

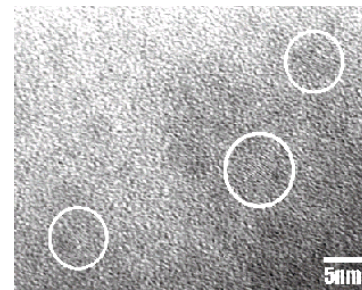

Fig. 3. High-resolution cross-sectional TEM image. The white boundaries in the figure are guides to the eyes.

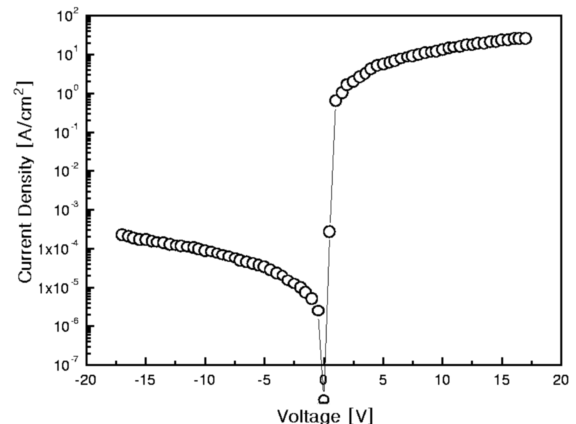

Fig. 4. Current density-voltage (J-V) characteristics of the EL device.

Torr throughout the present experiment. The flow rate of SiH_4 was 20 sccm, and the flow rates of N_2O were 32 sccm and 200 sccm for SRO and stochiometric SiO_2 layers, respectively. The growth temperature, T_g, was varied from 650 °C to 850 °C. The bonding configurations in the oxide matrix were measured by using a fourier transform infrared spectroscopy (FTIR, Biorad Excalibur FTS-3000).

The growth times of the SRO and the SiO_2 layers were 2 min and 2.5 min, respectively. Prior to the deposition of 3 periods of the SRO/SiO_2 superlattice, rapid thermal oxidation for 1 min was done for thermal oxide growth on the Si wafer surface for a passivation. The substrate was a 3-inch p-type Si wafer with a resistivity of 1 $\sim$ 10 Ωcm. The superlattice was subsequently annealed at 1100 °C for 2 h in a N_2 atmosphere. During the high-temperature annealing procedure, the amorphous SRO/SiO_2 superlattice transformed to a nanocrystal Si/SiO_2 superlattice. Au dots were evaporated using a shadow mask; an etching by diluted HF followed. Due to the thick Au dots, EL emission was allowed only from the etched sidewall of the superlattice.

Photoluminescence (PL) were excited by using the 488-nm line of an Ar^+-ion laser (30 mW and $\sim$ 1-mm beam diameter). The PL was dispersed by using a 0.5-m monochrometer (Dongwoo optron DM500). The PL signal was detected with a photomultiplier tube (Hamamatsu R928) by using the conventional lock-in technique (Standford Research SR810) with a chopper frequency of 500 Hz. The EL from our device was guided via an optical fiber to the monochrometer. The cross-sectional transmission electron microscope (TEM) measurement was made by using a JEOL JEM-2010 and a standard preparation technique. The devices were tested only under a DC bias condition.

III. RESULTS AND DISCUSSION

The growth of a stoichiometric SiO_2 layer is a prerequisite for SRO/SiO_2 superlattice fabrication. the SiO_2 layer is deposited with $[N_2O]/[SiH_4]$ = 50 at T_g = 850 °C. Figure 1 shows the FTIR spectra of the SRO and the SiO_2 layers. The position and the shape of Si-O-Si asymmetric stretching mode vibration are important for evaluating the stoichiometry of SiO_2 [17]. The Si-O-Si stretching mode shifts linearly with the oxygen content in the SRO layer [18]. The width of Si-O-Si stretching mode band decreases with increasing oxygen content in the layer due to a decrease in the randomness of Si-O bonding. Eventually, in the case of the SiO_2 layer, the Si-O-Si stretching mode band develops into a sharp

Fig. 5. Photograph showing orange-colored EL emission.

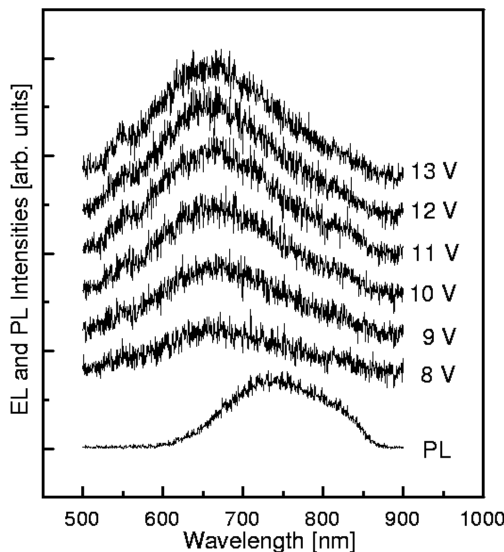

Fig. 6. EL spectra as a function of applied bias. For comparison, the PL spectrum is shown. Spectra are shifted for clarity.

peak with a shoulder. The shoulder is attributed to an out-of-phase vibration. In Fig. 1, the observed Si-O-Si stretching mode band for the SiO_2 layer is comparable to that of high-quality SiO_2 grown by dry oxidation. Thus, the FTIR spectra prove that the growth of a stoichiometric SiO_2 layer is possible. The growth conditions for RTCVD are fairly moderate compared to those for dry/wet oxidation.

Figure 2 shows a cross-sectional TEM image obtained using the defocus method at low magnification. The SRO layers appear as darker bands compared to the SiO_2 layers. The thicknessess of the SRO and the SiO_2 layers are 8 nm and 4 nm, respectively, which are close to the designed thicknesses. Due to a small difference in the material density, obtaining the lattice fringe of the nanocrystals in the defocus method is difficult. Figure 3 shows a high resolution cross-sectional TEM image. We observe several Si nanocrystals with sizes ranging from 3 to 5 nm.

Figure 4 show the current density-voltage (J-V) characteristics of our EL device. The J-V characteristics show the conventional rectification behavior of a diode.

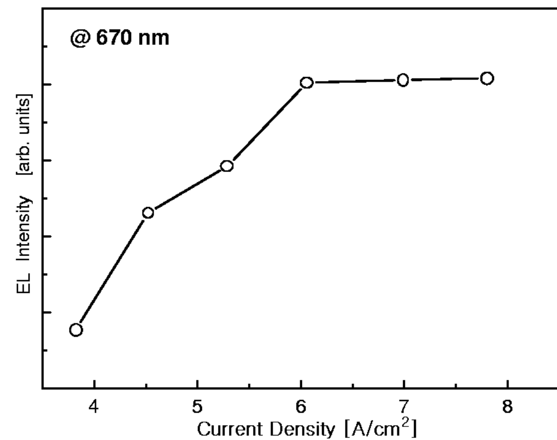

Fig. 7. EL intensity measured at 670 nm as a function of injection current.

The saturated current density ratio from the forward and the reverse bias regions is more than 10^5. The saturated current density under forward bias is $\sim$ 30 A/cm^2.

In some previous reports, significant current flowed through the device in reverse bias when employing a low resistivity Si substrate [14]. In this case, EL was also observed in reverse bias. We tried to measure the EL emission both under forward and reverse bias. However, EL emission was obtained only under forward bias. Figure 5 shows a photograph with orange EL emission, which is easily detectable with the naked eye under room-illumination conditions.

Figure 6 shows EL spectra and the PL spectrum of our device. There is significant blueshift of the EL spectra compared to the PL spectrum. The shift of EL observed at 8 V ($\sim$ 1.1 MV/cm) is $\sim$ 70 nm compared to the PL. Among the EL spectra, a systematic blueshift with increasing applied bias is found. The overall features in the EL spectra are fairly similar to those of a previous report by Photopoulos and Nassiopoulou [15]. Such features were explained in terms of Auger recombination, Coulomb charging effects, and/or the quantum-confined Stark effect. However, the trends we observed are in contrast with those reported by Franzo *et al.* [14]. In their report, there was no difference between the EL and the PL positions. In addition, they observed systematic broadening of the lower energy side of the EL spectra with increasing applied bias. In spite of the broadening, no shift of EL peak position was observed. It is noteworthy that the active layer of their device was a single SRO layer containing Si nanocrystals. In such a case, there would be significant size dispersion of Si nanocrystals. Furthermore, Si nanocrystals were randomly precipitated in the matrix. In our case, similar to the device of Photopoulos and Nassiopoulou, size dispersion is suppressed due to the superlattice structure, and the nanocrystals experience similar electric fields. The discrepancy between the EL and the PL peak positions may be a consequence of different radiative transitions.

For instance, the observed EL may be attributed to a defect-related transition. However, as observed by Bae *et al.* [19], matrix-defect-related PL is usually observed at ~ 450 nm. Furthermore, matrix-defect-related EL has a redshift rather than a blueshift. In addition, according to Photopoulos and Nassiopoulou [15], the amount of blueshift of EL compared to PL is ~ 60 nm for ~ 2-nm Si nanocrystals. Therefore, the 70-nm blueshift observed in the present experiment can be explained in terms of an orgin similar to that are discussed by Photopoulos and Nassiopoulou.

As Fig. 7 shows, the EL intensity measured at 670 nm increases with increasing bias and is saturated over 11 V. This means that further increases in the applied bias will result in overheating of our EL device. Neither a significant degradation nor an EL spectral shift were found when operating under 10 V.

IV. CONCLUSION

We have fabricated an EL device with a turn-on voltage as low as 8 V. The EL device employs a simple MOS diode with a nanocrystal Si/SiO_2 superlattice grown by using RTCVD. We have demonstrated that RTCVD is useful for preparing ultra-thin superlattice structures for efficient EL-device fabrication. the EL spectra show a systematic blueshift with increasing applied bias. By proper optimization of the device structure, a further reduction in the operating voltage and an increase in the EL efficiency are expected.

ACKNOWLEDGMENTS

This work was supported by the Dong-A University Research Fund in 2004.

REFERENCES

[1] L. T. Canham, Appl. Phys. Lett. **57**, 1046 (1990).
[2] S-H. Choi, B-Y. Seo, H. Lee, B. I. Hong, H. J. Lee and J. H. Lee, J. Korean Phys. Soc. **40**, 148 (2002).
[3] J. K. Kim, H. J. Cheong, K. H. Park, Y. Kim, J-Y. Yi and H. J. Bark, J. Korean Phys. Soc. **42**, S316 (2003).
[4] K. S. Min, Ph.D. dissertation, Caltech, 2000.
[5] F. Iacona, G. Franzo and C. Spinella, J. Appl. Phys. **87**, 1295 (2000).
[6] S. Lombardo and S. U. Campisano, Mat. Sci. Eng. R **17**, 281 (1996).
[7] M. Zacharias, J. Heitmann, R. Scholz, U. Kahler, M. Schmidt and J. Blasing, Appl. Phys. Lett. **80**, 661 (2002).
[8] M. Fujii, S. Hayashi and K. Yamamoto, Jpn. J. Appl. Phys. **30**, 687 (1991).
[9] L. Patrone, D. Nelson, V. I. Safarov, M. Sentis, W. Marine, and S. Giorgio, J. Appl. Phys. **87**, 3829 (2000).
[10] J. H. Shin, H. S. Han, S. Y. Seo and W. H. Lee, J. Koean Phys. Soc. **34**, S16 (1999)
[11] C. Y. Chang and S. M. Sze, *ULSI Technology* (McGraw-Hill, New York, 1996), Chap. 4.
[12] J. F. Gibbons, C. M. Gronet and K. E. Williams, Appl. Phys. Lett. **47**, 721 (1986).
[13] H. J. Cheong, J. H. Kang, J. K. Kim, Y. Kim, J-Y. Yi, T. H. Chung and H. J. Bark, Appl. Phys. Lett. **83**, 2922 (2003).
[14] G. Franzo, A. Irrera, E. C. Moreira, M. Miritello, F. Iacona, D. Sanfilippo, G. Di Stefano, P. G. Fallica,and F. Priolo, Appl. Phys. A **74**, 1 (2002).
[15] P. Photopoulos and A. G. Nassiopoulou, Appl. Phys. Lett. **77**, 1816 (2000).
[16] A. Irrera, D. Pacifici, M. Miritello, G. Franzo, F. Priolo, F. Iacona, D. Sanfilippo, G. Di Stefano and P. G. Fallica, Appl. Phys. Lett. **81**, 1866 (2002).
[17] G. Lucovsky, M. J. Manitini, J. K. Stivastava and E. A. Irene, J. Vac. Sci. Technol. B **5**, 530 (1987).
[18] P. G. Pai, S. S. Chao, Y. Takagi and G. Lucovsky, J. Vac. Sci. Technol. A **4**, 689 (1986).
[19] H. S. Bae, T. G. Kim, C. N. Whang, S. Im, J. S. Yun and J. H. Song, J. Appl. Phys. **91**, 4078 (2002).